Neutronics Shielding Analysis for the End Plug of a Tandem Mirror Fusion Reactor

M. Ragheb and C.W. Maynard

January 1981

UWFDM-398

FUSION TECHNOLOGY INSTITUTE

UNIVERSITY OF WISCONSIN

MADISON WISCONSIN

Neutronics Shielding Analysis for the End Plug of a Tandem Mirror Fusion Reactor

M. Ragheb and C.W. Maynard

Fusion Technology Institute
University of Wisconsin
1500 Engineering Drive
Madison, WI 53706

http://fti.neep.wisc.edu

January 1981

UWFDM-398

DOE/ET52048-14
UC-20

Neutronics Shielding Analysis for the End Plug of a Tandem Mirror Fusion Reactor

Magdi M. H. Ragheb*

and

Charles W. Maynard

January 1981

Fusion Engineering Program
Nuclear Engineering Department
The University of Wisconsin
Madison, Wisconsin 53706

UWFDM-398

(Please address correspondence to the first author.)

*Nuclear Engineering Program
The University of Illinois
Champaign-Urbana, Illinois 61801

Contents

Abstract

A neutronics analysis using the Monte Carlo method is carried out for the end-plug penetration and magnet system of a tandem mirror fusion reactor. Detailed penetration and magnet three-dimensional configurations are modelled. A method of position dependent angular source biasing is developed to adequately sample the DT fusion source in the central cell region and obtain flux contributions at the penetration components.

To assure cryogenic stability, the barrier cylindrical solenoid is identified as needing substantial shielding of about one meter of a steel-lead-boron carbide-water mixture. Heating rates there would require a thermal-hydraulic design similar to that in the central cell blanket region. The transition coils, however, need a minimal 0.2 m thickness shield. The leakage neutron flux at the direct convertors is estimated at 1.3×10^{15} $n/m^2 \cdot s$), two orders of magnitude lower than that reported at the neutral beam injectors for tokamaks (around 10^{17} $n/(m^2 \cdot s)$ for a 1 MW/m^2 14 MeV neutron wall loading). This result is obtained through a coupling between the nuclear and plasma physics designs in which hydrogen ions rather than deuterium atoms are used for energy injection at the end plug, to avoid creating a neutron source there. This lower and controllable radiation leakage problem is perceived as a potential major advantage of tandem mirrors compared to tokamaks and laser reactor systems.

I. Introduction

The present work is concerned with the neutronics shielding aspects of the barrier regions and end plugs of a tandem mirror reactor (TMR).

The WITAMIR-I conceptual design is a D-T fusion cycle TMR which aims at maximizing Q (the ratio of the fusion energy to the injected energy), to a value of 28, while retaining the features of a near term commercial reactor of 3000 MW of DT fusion power (1530 MWe). Both radiofrequency and neutral beam injection plasma heating are used, as well as direct conversion of ion energy to electricity. The potential for steady state operation, the much simpler blanket/shield and central cell coil design (compared to tokamaks), and the potential of burning advanced fuels such as D-D and D-^{3}He, are some of the attractive features of TMRs.[1] As shown in Fig. 1, the system comprises a central cell surrounded by solenoidal magnets and end plugs consisting of magnets of complex geometrical configurations. Neutral beam injection and radiofrequency heating are done outside the central cell. This is a major advantage from the shielding point of view compared to other fusion concepts. In the TMR case, the neutral beam injectors and the radiofrequency heating ducts will not be in direct line of sight of the central cell fusion plasma neutrons and as shown in Fig. 2, the D-T reaction reaches a zero value at the center of the end plug. The barrier cell will have a less intense source which will irradiate the heating units for this region. Injection of D into the end plug as is used in a previous design[2] for plasma heating is intentionally avoided in favor of H ion injection heating. This eliminates significant DD and DT neutron production at these positions, and avoids serious neutron leakage through plasma heating penetrations, a problem that is generic to other fusion concepts. For example, Jung and Abdou[3] report neutron

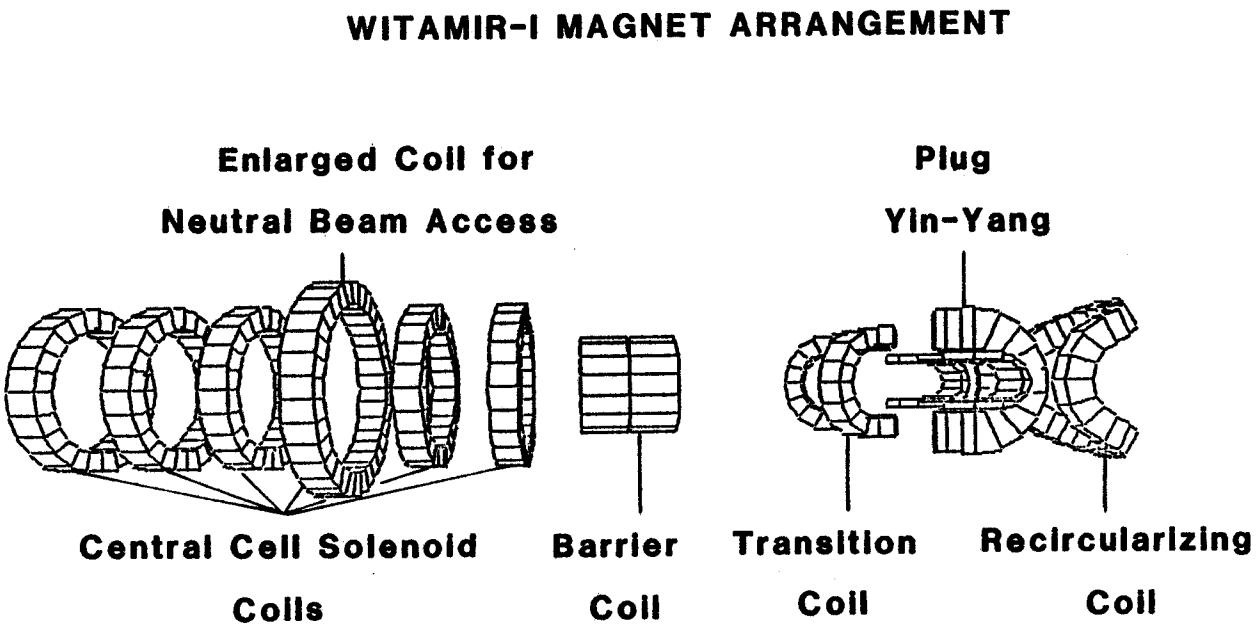

Figure 1. Barrier solenoid, end-plug, and central cell magnet system geometry.

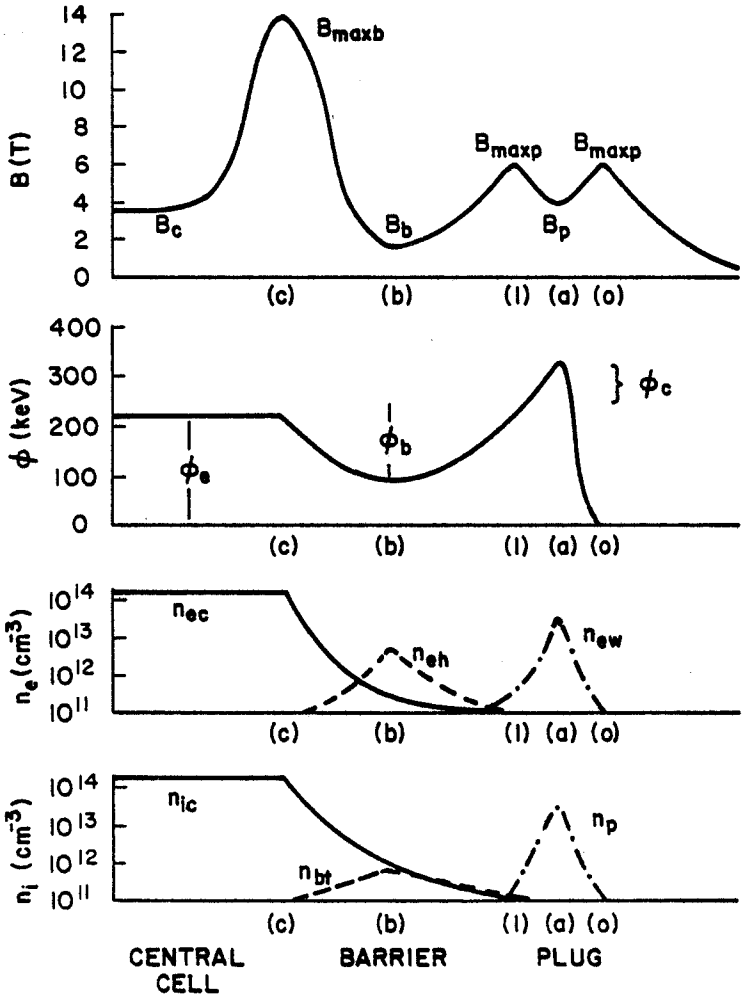

Figure 2. Magnetic and electrostatic fields and DT reaction distributions in tandem mirror reactor end-plug.

fluxes at the end caps of neutral beam injectors for a tokamak design of the order of 10^{17} $(n/m^2 \cdot s)$ for a 1 MW/m^2 14 MeV neutron energy wall loading. Ragheb, Klein, and Maynard[4,5] report neutron fluxes of the order of 10^{14} $(n/m^2 \cdot s)$ after the second beam reflection in a laser-driven ICF reactor. The latter flux is estimated to lead to a 10^6 rem/hr neutron dose rate at this position for a 14 MeV neutron source strength of 10^{21} (n/s).

In spite of this advantage, the end plug in the TMR is still subjected to neutron bombardment by neutrons born in the central cell portion of the reactor. In particular, the barrier cylindrical solenoid will need adequate shielding against these oncoming neutrons. The yin-yang, transition and recircularizing coils will also be subjected to leaking neutrons. The direct convertor at the end of the end plugs will see both line of sight and scattered neutron radiation from the central cell. The present study was undertaken to quantify the radiation shielding and leakage problems in the end plug of a typical TMR. To deal with the complexity of the three-dimensional geometrical configurations, Monte Carlo was used for the treatment of the problem. The MORSE Monte Carlo Code was used[6], as well as cross section data sets by Ford III et al.[7] and Abdou et al.[8] The geometrical model will be exposed in Sec. II including an analysis of a method of position dependent angular source sampling that was developed to adequately sample the central-cell neutron source. Results of calculations are discussed in Sec. III.

II. Calculational Model

II-1. Geometrical Configurations and Material Compositions

Figure 3 shows the actual geometry in the end plug, and Fig. 4 the geometrical model adopted for the calculations. Because of symmetry, half the

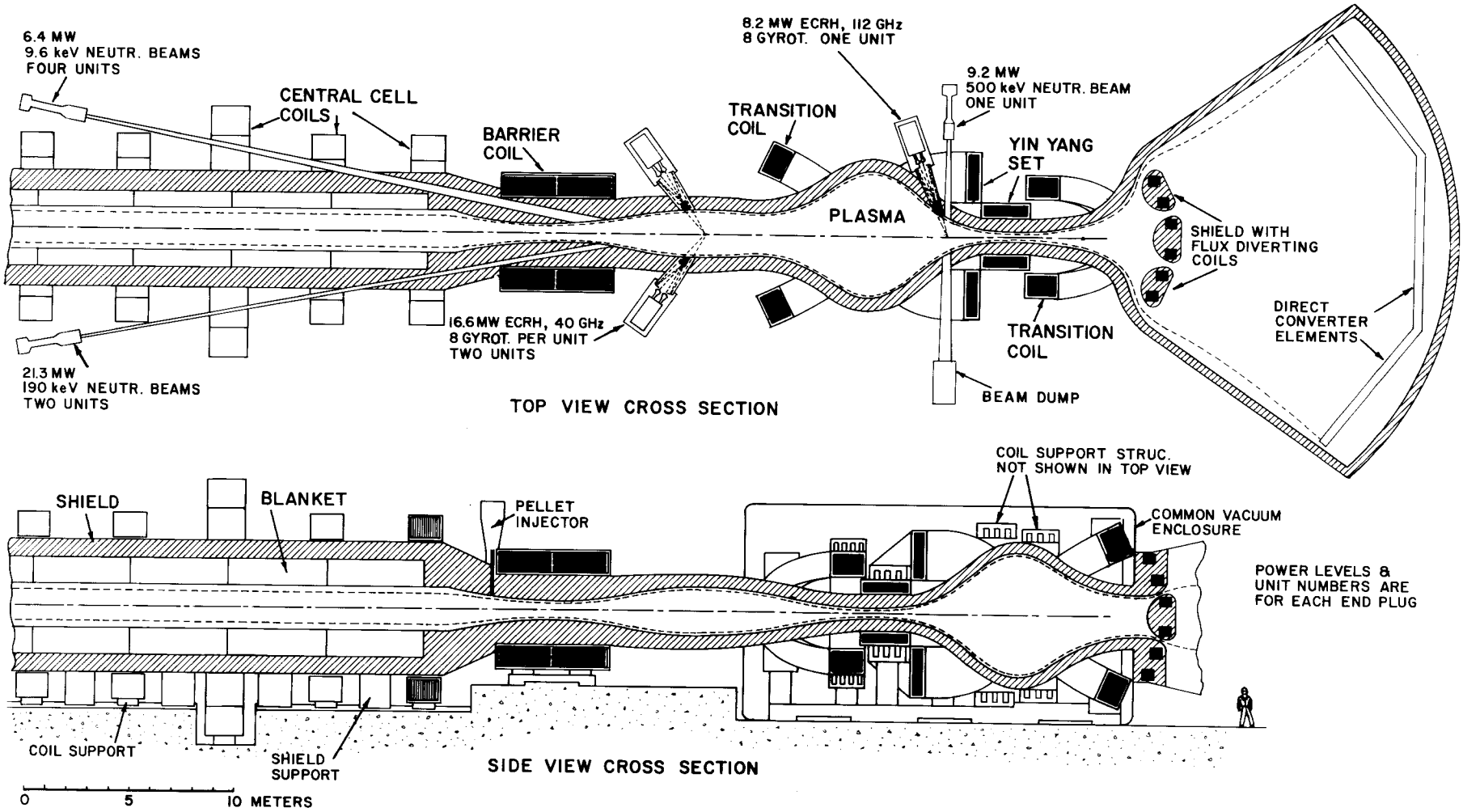

Figure 3. Actual end-plug geometry.

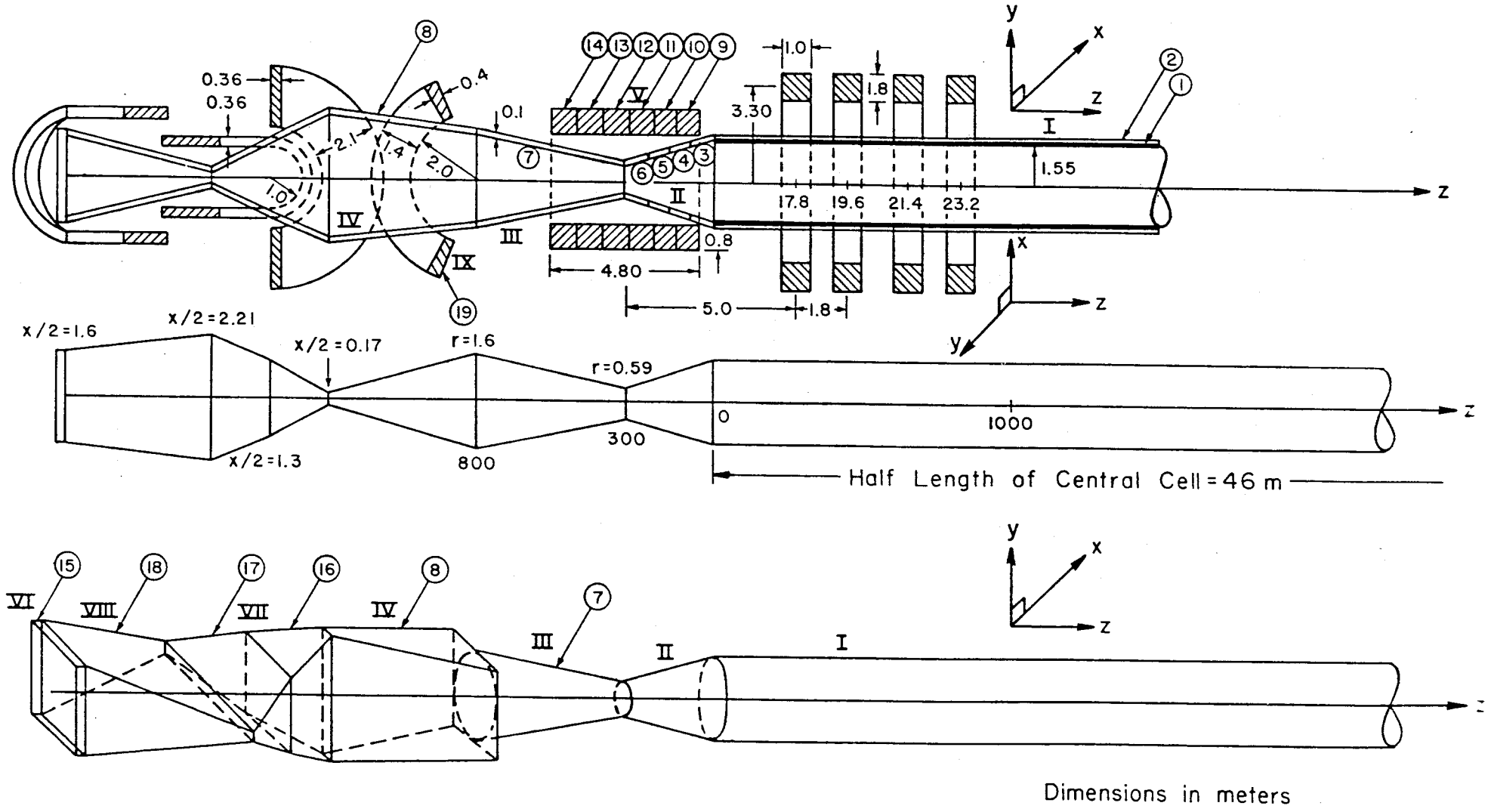

Figure 4. Geometry of calculational model for end-plug cavity.

central cell is considered in the calculation with a reflecting boundary condition at its center. The half length of the central cell is 46 m and the plasma radius is 1.35 m. A clearance of 0.2 m was left between the plasma and the first wall. The blanket (region I) was divided into two zones 1 and 2 of 0.1 and 0.653 m, respectively. The entire end plug penetration was surrounded by a 0.1 m penetration shield thickness with the composition in Table I, and having the shape shown in Fig. 4. This shield is constricted in a conical shape inside the cylindrical solenoid and is divided for estimation purposes into four zones 3, 4, 5, and 6 in its converging part (II), and one zone 7 in its diverging part (III). The cylindrical solenoid (V) is divided into six detector zones: 9-14. Its composition is a homogenization of magnet materials as shown in Table I.

The penetration shield for the front transition coil (IV) is designated as zone 8, and takes the form of a parallelepiped that starts with a wide base and then is constricted to a thin slit of 0.34 m width and 4.42 m length. Through this slit the magnetic field lines take the form of a fan and enter the yin-yang coil region (VII). In this region the penetration shield is divided into two zones 16 and 17. The end part shield for the second recircularizing coil is designated as region VIII (zone 18). To quantify the neutron leakage from the system, the penetration is ended by an end plug slab (VI) of the same material as the penetration shield. Notice that the penetration shield undergoes two perpendicular squeezes into thin slits so that the end slab sees in direct line of sight a small solid angle of the central cell neutron source.

The first transition coil is modelled in its exact dimensions as shown in Fig. 5 and is designated as region IX (zone 19).

Table I

Material Compositions and Elemental Mixes Used in Calculations

Region	Composition	Nuclide Density [atoms/barn.m)] x 10^{-2}
I. Blanket	Pb	2.381-02
90v/o $Li_{17}Pb_{83}$ Breeder and Coolant	^{7}Li	4.512-03
+ 10v/o Ferritic Steel (11 w/o Cr	^{6}Li	3.658-04
+ 89 w/o Fe)	Fe	7.678-03
	Cr	1.019-03
II. Shield	Fe	4.607-02
60v/o Ferritic Steel + 15v/o Pb	Cr	6.115-03
+ 15v/o B_4C + 5v/o H_2O	Pb	4.945-03
	^{10}B	3.270-03
	^{11}B	1.308-02
	^{12}C	4.087-03
	^{1}H	3.337-03
	^{16}O	1.668-03
III. Magnets	^{27}Al	3.629-02
60v/o Al + 30v/o Cu + 10v/o He	Cu	2.547-02
	^{4}He	1.836-03
IV. First Wall	Fe	7.678-02
Ferritic Steel (11 w/o Cr	Cr	1.019-02
+ 89 w/o Fe)		
V. Reflector	Fe	7.294-02
95v/o Ferritic Steel	Cr	9.682-03
+ 5v/o H_2O Coolant	^{1}H	3.337-03
	^{16}O	1.668-03

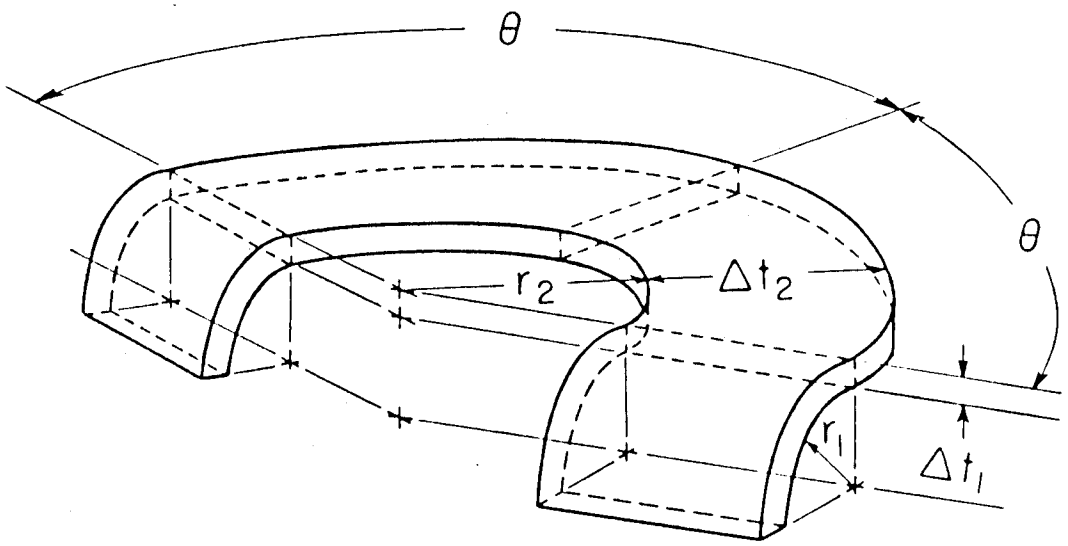

$\theta = 65°$

$r_1 = 2.00, \quad \Delta t_1 = 0.4$

$r_2 = 2.00, \quad \Delta t_2 = 1.4$

Figure 5. Geometry of one of the transition coils.

We concentrate our attention in the present work on developing the methodology to adequately sample the central cell neutron source as shown in the next subsection and study its effect on the end part of the penetration, in particular the constriction part (region II), recirculatizing (IX), and cylindrical (V) coils, as well as the leakage from the system at the slab plug (VI). These are the parts to be most affected by the central cell neutron source. Future studies will also have to consider the yin-yang coils and the second recirculatizing coil, and the contribution to the neutron production (even though much smaller than in the central cell) at the barrier region (regions II, III, and IV).

II-2. Position Dependent Angular Source Biasing

The total DT fusion power of the reactor is P_f = 3000 MW. This corresponds to a source strength of:

$$S = \frac{P_f C}{17.62} \times 10^6 \frac{[14 \text{ MeV neutrons}]}{\text{second}} \qquad (1)$$

where C is a conversion factor of Joules to MeV (0.62418×10^{13}). Substituting for the different factors we get: $S = 1.063 \times 10^{21}$ (n/sec). This corresponds to a 14.1 MeV neutron wall loading of:

$$3000 \times \left(\frac{14.1}{17.62}\right) \times \frac{1}{2\pi(1.55)92} = 2.68 \text{ MW/m}^2 \quad .$$

Our flux estimates will be given in units of [n/m^2 · source particle] so that absolute flux values can be obtained by multiplying by $S \cdot \Delta\Omega/4\pi$ to get the fluxes in units of [n/m^2 sec]. We considered one quadrant of the geometry in our modeling so that $\Delta\Omega/4\pi = 1/8$.

The first column of Table II shows that sampling the neutron source uniformly and isotropically in the central cell fails to lead to any flux estimates at the end parts of the penetration and at the first recirculating coil, even when larger numbers of histories were used. Thus it was necessary to develop the technique of position dependent angular source biasing as explained below. The technique is an extension of the well-known method of angular source biasing, where the angular biasing of a source particle will depend on its position in the penetration.

First an axial position z is sampled uniformly along half the penetration length from the distribution function:

$$p(z) = \frac{dz}{\int_o^L dz} = \frac{dz}{L} \quad . \tag{2}$$

(We experimented with biased source position sampling with an isotropic source without the same improvement effect as in the case of angular source biasing.)

Second, the solid angle subtended by the penetration end from that position z is calculated as:

$$\Omega = \int d\Omega = \int \frac{ds}{r^2} = \int \frac{r^2 \sin\theta d\theta d\phi}{r^2} \, 2\pi \, (1-\cos\theta_1).$$

Writing down the expression for cos θ_1 in terms of the penetration radius R, cell length L (see Fig. 6), and axial position z, we get:

$$\Omega = 2\pi \left[1 - \frac{1}{\sqrt{1+(\frac{R}{L-z})^2}}\right] \quad . \tag{3}$$

Table II

Scalar Neutron Fluxes [n/m^2 · source particle] x 10^{-4}

For Isotropic and Forward Biased Source

Sampling in Different Reactor Regions (2000 histories)

Region	Zone	Isotropic Uniform Source in Central Cell	Forward Biased, Uniform Source in Central Cell
I. Blanket Central Cell	1	2.5771-05(0.027)*	3.7952-05(0.096)
	2	8.7237-06(0.009)	6.6793-06(0.091)
II. Barrier Solenoid Front Shield	3	5.7600-06(0.154)	5.2856-06(0.174)
	4	4.9386-06(0.160)	3.1065-06(0.233)
	5	4.1473-06(0.218)	2.3040-06(0.197)
	6	3.0498-06(0.202)	2.5236-06(0.273)
III. Barrier Solenoid Back Shield	7	1.9361-07(0.240)	1.1663-07(0.307)
IV. Transition Coil Shield	8	5.5724-08(0.439)	3.1038-08(0.760)
V. Barrier Solenoid	9	6.5995-07(0.269)	1.2934-07(0.314)
	10	3.4467-07(0.374)	1.5548-07(0.294)
	11	7.0234-08(0.469)	1.9865-07(0.378)
	12	9.6962-08(0.830)	9.4308-08(0.520)
	13	9.2967-08(0.720)	3.9598-08(0.685)
	14	2.0241-08(0.573)	3.7901-09(0.924)
VI. Penetration Plug	15	-	1.7648-09(0.592)
VII. Yin-Yang Coil Shield	16	-	3.9392-09(0.722)
	17	-	5.5289-09(0.924)
VIII. End Part Shield	18	-	1.3640-10(0.570)
IX. Transition Coil	19	-	4.0982-10(0.922)

*Numbers in parentheses are fractional standard deviations.

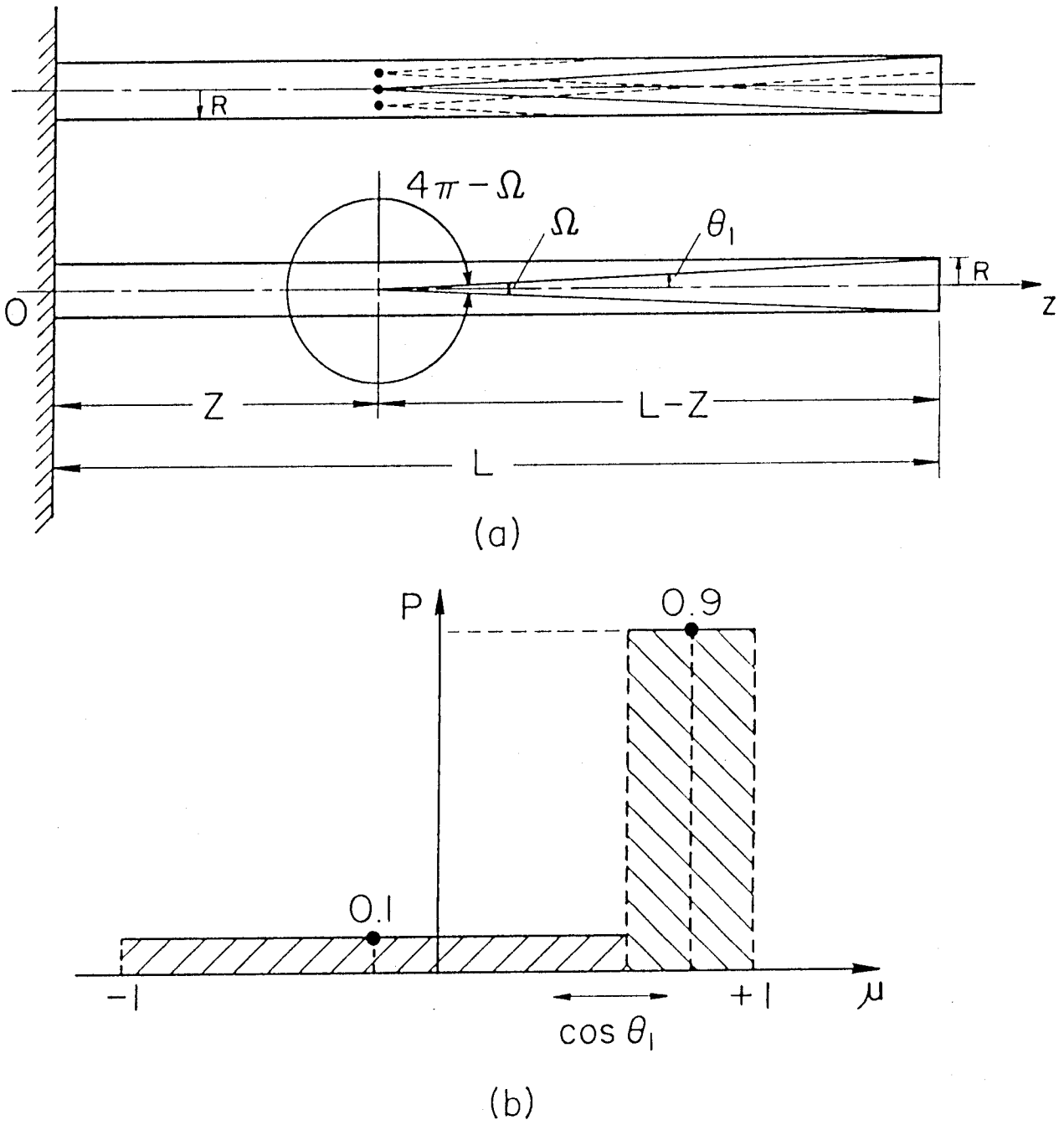

Figure 6. Position dependent angular source biasing.

For an isotropic source, the probability of a particle emerging within Ω is:

$$p_1 = \frac{\Omega}{4\pi} \tag{4}$$

and the probability of a particle emerging in the solid angle $(4\pi-\Omega)$ will in turn be:

$$p_2 = 1 - p_1 = 1 - \frac{\Omega}{4\pi} \quad . \tag{5}$$

One can assign arbitrary probabilities p_1' and p_2', for particle births in either Ω or $(4\pi-\Omega)$ solid angles, provided their statistical weights w_1 and w_2 are adjusted according to:

$$\left.\begin{aligned} p_1' \, w_1 &= p_1 \\ p_2' \, w_2 &= p_2 \end{aligned}\right\} \tag{6}$$

such that:

$$p_1' + p_2' = 1 \quad .$$

Substituting from Eqs. 4 and 5 into Eq. 6, we get:

$$w_1 = \frac{\Omega}{4\pi} \cdot \frac{1}{p'_1}$$

$$w_2 = (1 - \frac{\Omega}{4\pi}) \cdot \frac{1}{p'_2} \quad . \qquad (7)$$

As an example, if $\Omega = 2\pi$, with $p'_1 = 1$ and $p'_2 = 0$; implying $w_1 = 0.5$, this is a case of forward source biasing. If $p'_1 = 0.9$ and $p'_2 = 0.1$, then the source particle weights would be $w_1 = \frac{2\pi}{4\pi} \cdot (1/0.9) = 0.5555$, and $w_2 = \frac{2\pi}{4\pi} \cdot \frac{1}{0.1} = 5.0$. In both cases the probabilities $p_1 = p_2 = 0.5$ are preserved.

In our calculations, we experimented with several values of p'_1 and p'_2 and chose $p'_1 = 0.9$ and $p'_2 = 0.1$. This choice leads to particles reaching the reactor extremities without collision 90% of the time and particles suffering at least one collision before reaching these zones 10% of the time. In this way, contributions from all particles will still be obtained. This is thought better than considering purely forward source biasing without the other component. Figure 6 shows these choices of the cosine of the angle θ, where direct particles are favored with respect to indirect particles. In this case the source statistical weight adjustment for direct and indirect moving particles will be respectively:

$$w_1 = \frac{1}{2} \left[1 - \frac{1}{\sqrt{1+(\frac{R}{L-z})^2}}\right] \cdot \frac{1}{p'_1} \qquad (8)$$

$$w_2 = 1 - \left[1 - \frac{1}{\sqrt{1+(\frac{R}{L-z})^2}}\right] \cdot \frac{1}{p'_2}$$

by use of Eqs. 3 and 7.

A radius is then sampled for the source particle from the distribution function:

$$p(r)dr = \frac{2\pi r dr}{\int_0^R 2\pi r dr} = \frac{2r dr}{R^2} \tag{9}$$

and an azimuthal angle from the distribution function:

$$p(\phi)d\phi = \frac{d\phi}{\int_0^{\frac{\pi}{2}} d\phi} = \frac{2d\phi}{\pi} \tag{10}$$

where we are using one quadrant of the geometry with reflecting boundaries to account for symmetry.

The last step in the source sampling is the sampling of the polar angle. For direct directions this is sampled using the distribution function:

$$\rho(\phi) = \frac{2\pi \sin\theta \, d\theta}{2\pi \int_0^{\theta} 1 \sin\theta \, d\theta} \tag{11}$$

which samples isotropic vectors within the conical half angle:

$$\theta_1 = \cos^{-1}\left[\frac{(L - z)}{\sqrt{R^2 + (L - z)^2}}\right] .$$

In the same way for indirect directions,

$$p(\theta) = \frac{2\pi \sin\theta \, d\theta}{2\pi \int_{\theta_1}^{\pi} \sin\theta \, d\theta} . \tag{12}$$

Where the above methodology is applied, contributions to different parts of the end plug penetration can now be obtained as shown in Table II, even for small numbers of particle histories (2000 histories). In the next section we discuss the application of the developed methodology to obtain quantities of interest in the penetration.

III. Discussion of Results

III-1. Scalar Flux Distributions

The methodology developed in the last section succeeds in obtaining estimates in the end plug penetration caused by the central cell neutron source. Table III shows these results and their corresponding standard deviations for 2000 and 8000 particle histories, for a penetration shield thickness of 0.1 m.

For the case of 8000 histories, at the penetration plug (region VI) we get an estimate of the flux with 36% fractional standard deviation which is quite good for our type of survey calculations. Using the source strength estimate for this particle design from section II.2, we can estimate the leakage neutron flux as:

$$\frac{1.063 \times 10^{21}}{8} \times 9.8492 \times 10^{-10} \times 10^{+4} = 1.31 \times 10^{15} (n/m^2 \cdot s)$$

where the division by the factor 8 accounts for using one quadrant of the geometry in our modeling. This identifies the need for adequate shielding at the end of the penetration to avoid serious activation of the charged particle direct-energy convertor beyond this point. As shown in Table IV, the contribution to the scalar flux there is $\frac{4.7178 \times 10^{-11}}{9.8419 \times 10^{-10}} \approx 5\%$ from direct line of sight 14 MeV neutron radiation, the rest being intermediate energy group

Table III

Effect of Increasing the Number of Histories
on the Flux Estimates in the Central Cell and End Plug of the TMR.
Uniformly Distributed, Forward Biased Source in Central Cell.
$[n/m^2 \cdot \text{source particle})] \times 10^{-4}$
Effective Penetration Shield Thickness = 0.1 m.

Region	Zone	2000 Histories	8000 Histories
I. Blanket Central Cell	1	3.7952-05(0.096)*	4.1262-05(0.043)
	2	6.6793-06(0.091)	7.7188-06(0.043)
II. Barrier Solenoid Front Shield	3	5.2856-06(0.174)	5.2437-06(0.085)
	4	3.1065-06(0.233)	4.8442-06(0.099)
	5	2.3040-06(0.197)	3.7601-06(0.124)
	6	2.5236-06(0.273)	2.3820-06(0.147)
III. Barrier Solenoid Back Shield	7	1.1663-07(0.307)	1.4502-07(0.227)
IV. Transition Coil Shield	8	3.1038-08(0.760)	3.4541-08(0.276)
V. Barrier Solenoid	9	1.2934-07(0.314)	2.4778-07(0.185)
	10	1.5548-07(0.294)	2.0933-07(0.250)
	11	1.9865-07(0.278)	1.9423-07(0.230)
	12	9.4308-08(0.520)	7.6307-08(0.318)
	13	3.9598-08(0.685)	4.8229-08(0.352)
	14	3.7901-09(0.924)	3.4796-09(0.404)
VI. Penetration Plug	15	1.7648-09(0.592)	9.8492-10(0.360)
VII Yin-Yang Coil Shield	16	3.9392-09(0.722)	2.0527-09(0.615)
	17	5.5289-09(0.570)	3.1262-09(0.655)
VIII. End Part Shield	18	1.3640-10(0.570)	7.2900-11(0.333)
IX. Transition Coil	19	4.0982-10(0.922)	3.4235-09(0.825)

*Numbers in parentheses are fractional standard deviations

Table IV

Total, Thermal, and 14 MeV Group Neutron Flux Components in Different TMR Regions. Effective Penetration Shield Thickness = 0.2 m. Number of Particle Histories: 8000. [n/(m^2·source particle)] x 10^{-4}.

Region	Zone	Total Scalar Flux	Thermal Group Flux	14 MeV Group Flux
I. Blanket Central	1	4.0225-05	9.4417-11	8.3862-07
Cell	2	7.6330-06	1.7644-11	3.3045-08
II. Barrier Solenoid	3	4.6877-06	2.1065-12	1.9958-07
Front Shield	4	3.1426-06	7.8637-12	9.0889-08
	5	2.0096-06	2.3138-12	3.4453-08
	6	1.1431-06	3.4976-12	8.5859-09
III. Barrier Solenoid	7	8.9974-08	4.7289-14	1.1205-10
Back Shield				
IV. Transition Coil	8	3.1736-08	1.3962-15	9.0361-11
Shield				
V. Barrier Solenoid	9	6.3143-08	1.2200-13	1.3733-11
	10	4.1566-08	3.3235-12	1.6357-12
	11	3.5821-08	8.0941-13	
	12	9.2307-09	1.8568-14	
	13	8.9983-09		
	14	6.9132-10		
VI. Penetration Plug	15	9.8419-10		4.7178-11
VII. Yin-Yang Coil	16	2.6279-12		1.6843-14
Shield	17	9.5934-10		2.3358-12
VIII. End Part Shield	18	4.5833-11		9.4176-13
IX. Transition Coil	19	1.0475-11		

components, since the thermal neutron components would have been absorbed along the penetration.

As previously done in a laser-fusion reactor[5] penetration the incorporation of boron in the material of the penetration liner would reduce this leakage, e.g., by use of Boral. The use of a flux trap at this point seems also necessary at the location of the penetration as suggested for a similar system in reference (5). The charged particles to the direct convertor can be bent using magnets as suggested by Moir, Barr and Miley[9], to let the neutrons fall into the flux trap.

A matter of previous concern was the tapered portion of the barrier solenoid shield. On the one hand, this part sees the whole length of the central cell source in a line-of-sight manner, but on the other hand it sees the neutron source from one side only compared to a first wall point, which sees it from both sides so that an estimate of the flux was needed. Our calculations show that the flux there will be less than at the first 10 cm of the blanket in the central cell. In fact, from Table III, in zone 3 of the barrier solenoid front shield the scalar flux is: $\frac{5.2437 \times 10^{-6}}{4.1262 \times 10^{-5}} \approx 12.7\%$ of that at the first wall. From Table IV, the 14 MeV group flux ratio is $\frac{1.9958 \times 10^{-7}}{8.3862 \times 10^{-7}} \approx 23.8\%$.

The transitional coil (region IX) coil received an average flux of (multiplying the values of Table III for 8000 histories by the source strength):

$$\frac{1.063 \times 10^{21}}{8} \times 3.4235 \times 10^{-9} \times 10^{4} = 4.549 \times 10^{15} \ (n/m^2 \cdot s) \ .$$

This is substantial and means that the originally chosen penetration shield

thickness of 0.1 m is insufficient.

The effect of altering the material thickness of this penetration shield on neutron fluxes in the magnets surrounding the penetration will be studied by varying the effective optical thickness of the penetration shield rather than changing the actual geometry. This is achieved by modifying the macroscopic cross section by a factor n as:

$$\Sigma = n\Sigma_o = nN_o\sigma \tag{13}$$

where: Σ, Σ_o are the modified and original macroscopic cross sections[12], respectively,

N_o is the original nuclide density,

σ is the material microscopic cross section.

For an optical thickness of the original system:

$$\ell_o = \frac{t}{\lambda_o} = t \cdot \Sigma_o \tag{14}$$

where: t is the geometrical thickness,

λ_o is the original material mean free path,

the modified optical thickness will be (using Eqs. 13 and 14):

$$\ell = \frac{t}{\lambda} = t\ \Sigma = nt\Sigma_o = n\ell_o \quad . \tag{15}$$

Thus the complicated task of changing a complex three dimensional geometry can be replaced by the simple task of modifying the mixing of the cross section by a factor n multiplying the number densities of the materials in the code

input; this will lead to the increase of the optical thickness of a given region n times.

Table V shows the results of this type of calculation where the effective penetration thickness is increased for 0.1 m to 0.2 m by the use of n = 2 in Eq. 15. This increase in the shield thickness leads to about an order of magnitude attenuation of the scalar flux at the barrier solenoid (region V), and to two orders of magnitude attenuation at the first transition coil (region IX).

III-2. Estimated Required Penetration Shield Thickness

We use as a criterion for the magnet shielding that the limit on local nuclearly induced resistivity increase does not exceed 10% of the unirradiated value assuring cryogenic stabilization[11]. Cryogenic stabilization requires that the heat transfer from the stabilized conductor matrix must be sufficient to transfer the Joule (I^2R) heat generated in the stabilizing material when a flux jump occurs. Since the magnet conductor currents must remain constant, an increase in Joule (I^2R) heating will occur through an increase of conductor resistance. The consequences of superconducting magnets going normal in a fusion reactor are likely to be grave, due to the large amount of energy stored in them, and the activation radioactivity in the adjacent components. This makes stabilization of superconducting coils in fusion reactors an important consideration.

For Al and Cu at 20 K the resistivity is:

$$\rho_{Al} = 5.4 \times 10^{-5} \ \mu\Omega \cdot m \ ,$$

$$\rho_{Cu} = 7.7 \times 10^{-5} \ \mu\Omega \cdot m \ .$$

Table V

Effect of Doubling the Optical Thickness of the TMR End Plug Penetration Shield on Fluxes at Magnets (8000 Histories). [n/m^2·source particle] x 10^{-4}.

Region	Zone	Effective Shield Thickness (m)	
		0.10	0.20
I. Blanket Central Cell	1	4.1262-05(0.043)*	4.0295-05(0.035)
	2	7.7188-06(0.043)	7.6330-06(0.031)
II. Barrier Solenoid Front Shield	3	5.2437-06(0.085)	4.6877-06(0.090)
	4	4.8442-06(0.099)	3.1426-06(0.104)
	5	3.7601-06(0.124)	2.0096-06(0.115)
	6	2.3820-06(0.147)	1.1431-06(0.191)
III. Barrier Solenoid Back Shield	7	1.4572-07(0.227)	8.9974-08(0.206)
IV. Transition Coil Shield	8	3.4541-08(0.276)	3.1736-08(0.276)
V. Barrier Solenoid	9	2.4778-07(0.185)	6.3143-08(0.411)
	10	2.0933-07(0.252)	4.1566-08(0.451)
	11	1.9423-07(0.230)	3.5821-08(0.774)
	12	7.6307-08(0.318)	9.2307-09(0.496)
	13	4.8229-08(0.352)	8.9983-09(0.777)
	14	3.4796-09(0.404)	6.9132-10(0.728)
VI. Penetration Plug	15	9.8492-10(0.360)	9.8419-10(0.548)
VII. Yin-Yang Coil Shield	16	2.0527-09(0.615)	2.6279-12(0.527)
	17	3.1262-09(0.655)	9.5934-10(0.977)
VIII. End Part Shield	18	7.2900-11(0.333)	4.5833-11(0.369)
IX. Transition Coil	19	3.4235-09(0.825)	1.0475-11(0.874)

*Numbers in parentheses are fractional standard deviations

The maximum allowable increase according to our stated criterion will be:

$$\delta\rho_{Al} = \frac{\rho_{Al}}{10} = 5.4 \times 10^{-6} \ \mu\Omega \cdot m$$

$$\delta\rho_{Cu} = \frac{\rho_{Cu}}{10} = 7.7 \times 10^{-6} \ \mu\Omega \cdot m \ .$$

An allowable flux level ϕ_a at the magnets can be calculated, as suggested by Lee in Ref. 2, from:

$$\phi_a = \frac{\delta\rho}{d\rho/d\psi} \ \frac{1}{t_r} \tag{16}$$

where: t_r is the required irradiation time (sec),

ψ is the neutron fluence (n/m^2),

$d\rho/d\psi$ is the slope of the relationship between ρ and ψ,[2]

$$\approx 2.210 \times 10^{-25} \ \frac{\mu\Omega \cdot m}{n/m^2} \quad \text{for Al,}$$

$$\approx 6.500 \times 10^{-26} \ \frac{\mu\Omega \cdot m}{n/m^2} \quad \text{for Cu.}$$

Annealing at room temperature produces 85% recovery in Cu and complete recovery in Al, even though the influence of cyclic irradiation is uncertain. Thus, if we want a one year time span between room temperature anneals of cyrogenic aluminum, the allowable flux level at the magnets must be:

$$\phi_a(Al) = \frac{5.4 \times 10^{-6}}{2.210 \times 10^{-25}} \times \frac{1}{3.154 \times 10^{7}} = 7.747 \times 10^{11} \ n/(m^2 \cdot s)$$

and for copper:

$$\phi_a(\mathrm{Cu}) = \frac{7.7 \times 10^{-6}}{6.5 \times 10^{-26}} \times \frac{1}{3.154 \times 10^{7}} = 3.760 \times 10^{12} \ \mathrm{n/(m^2 \cdot s)} \quad .$$

Since Al has a value of ϕ_a lower than that for Cu, for a conservative design, we use the value of ϕ_a for Al.

If we assume a flux attenuation of the form:

$$\phi = \phi_o \exp\left(-\frac{y - x}{2\lambda}\right) \tag{17}$$

where: λ is an attenuation mean free path,

ϕ and ϕ_o are assumed measured at the center of two penetration shield thicknesses y and x respectively, such that $y > x$;

then we can estimate a local flux attenuation coefficient from:

$$\lambda = \frac{y - x}{2 \ln (\phi_o/\phi)} \ (\mathrm{m}) \quad . \tag{18}$$

For $y = 0.2$ m, $x = 0.1$ m, as used in Table V, we can estimate local values for λ as shown in Table VI for the magnet regions of interest. Using these calculated values of λ, one can now calculate a shield thickness y for a given allowable flux ϕ_a from

$$y = x + 2\lambda \ln \frac{\phi_o}{\phi_a} \quad . \tag{19}$$

For the $x = 0.1$ m case results from Table V, values of the required penetration shield thicknesses are shown in Table VI.

Table VI

Required Penetration Shield Thicknesses to Attenuate Scalar Flux in Magnets to Allowable Limit:

$\phi_a(Al) = 7.747 \times 10^{11}$ n/m^2·s.

Region	Zone	$\phi_o(\frac{n}{m^2 \cdot s})$ x = 0.1 m	$\phi(\frac{n}{m^2 \cdot s})$ y = 0.2 m	λ(m) Local Attenuation Mean Free Path	Required Shield Thickness (m)
V. Barrier Solenoid	9	3.292+17	8.390+16	0.0366	1.05
	10	2.781+17	5.523+16	0.0310	0.89
	11	2.581+17	4.760+16	0.0296	0.85
	12	1.014+17	1.227+16	0.0235	0.65
	13	6.408+16	1.196+16	0.0298	0.77
	14	4.624+15	9.186+14	0.0310	0.64
IX. Transition Coil	19	4.549+15	1.392+13	0.0086	0.25

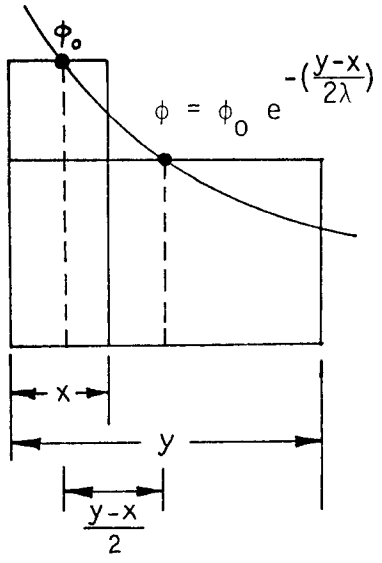

Based on the chosen criterion it appears that about 1.05 m of shield thickness will be sufficient to shield the cylindrical solenoid of the barrier coil, particularly its zone 9.

The shielding for the transition coil, however, needs only 0.247 m of shielding with the composition of Table I.

III-3. Heating Rates in Different Penetration Components

Table VII shows the heating rates due to neutrons both in units of MeV/source neutron, and as volumetric heating rates in units of MW/m^3. It can be noticed that the barrier solenoid shield has a high volumetric heating rate (5.8 MW/m^3) that is comparable to that at the central cell (8.1 MW/m^3). As a consequence this part of the shield will require a special thermal hydraulic design similar to that of the first wall/blanket region. The heating rate drops to low values in other parts of the penetration, and no substantial cooling is needed there. These estimates need to be supplemented by estimates of γ-ray heating for an exact determination of the nuclear heating. The sum of the total nuclear heating and the nuclear-induced I^2R heating through the increase in resistivity must then be made to be a fraction of the I^2R heating in the unirradiated coil, through adequate shielding.

In parts of the shield with low volumetric heating rates, low cost concrete or lead mortar shielding[4] can replace the more expensive steel, lead and boron carbide shielding mixture used in the present study.

III-4. Atomic Displacements and Gas Production Rates

The atomic displacement rates in units of displacements per atom per year are shown in Table VIII for the Al and Cu constitutents in the magnets for two thicknesses of the penetration shield of 0.1 m and 0.2 m. For comparison, the atomic displacement rates at the blanket first wall in the central cell are

Table VII

Heating Rates in Different Penetration Regions.

Effective Penetration Shield Thickness: 0.2 m.

Region	Zone	Volume $m^3 \times 10^{+6}$*	MeV Per Source Neutron	MW/m^3	Fractional Standard Deviation
I. First 0.1 m of Central Cell Blanket	1	1.160×10^{6}	4.431+00	8.132+00	0.033
	2	9.330×10^{7}	2.395+00	5.465-01	0.037
II. Barrier Solenoid Front Shield	3	1.418×10^{5}	3.836-02	5.759+00	0.075
	4	1.607×10^{5}	2.841-02	3.763+00	0.090
	5	1.311×10^{5}	1.582-02	2.569+00	0.106
	6	9.642×10^{4}	6.042-03	1.332+00	0.162
III. Barrier Solenoid Back Shield	7	9.020×10^{5}	4.897-03	1.156-01	0.165
IV. Transition Coil Shield	8	1.440×10^{6}	2.348-03	3.471-02	0.238
V. Barrier Solenoid	9	1.910×10^{6}	6.581-04	7.335-03	0.440
	10	1.910×10^{6}	3.959-04	4.413-03	0.416
	11	1.910×10^{6}	2.274-04	2.534-03	0.668
	12	1.910×10^{6}	8.692-05	9.688-04	0.509
	13	1.910×10^{6}	7.326-05	8.165-04	0.654
	14	1.910×10^{6}	3.057-06	3.407-05	0.707
VI. Penetration Plug	15	3.610×10^{5}	3.385-05	1.996-03	0.437
VII. Yin-Yang Shield	16	5.660×10^{6}	1.224-06	4.604-06	0.404
	17	5.660×10^{6}	2.752-04	1.035-03	0.974
VIII. End Part Shield	18	1.440×10^{6}	3.977-06	5.879-05	0.364
IX. Transition Coil	19	3.650×10^{6}	2.319-07	1.353-06	0.852

*Volumes pertain to one quadrant of the geometry.

Table VIII

Atomic Displacement Rates in Magnet Components (dpa/year)

Effective Penetration Shield Thickness = 0.2 m

Region	Zone	Al in Magnets	Cu in Magnets
Barrier Solenoid	9	1.477-01	8.192-02
	10	6.860-02	4.093-02
	11	4.311-02	2.803-02
	12	1.924-02	1.068-02
	13	2.927-03	2.623-03
	14	5.552-05	1.773-04
Transition Coil	19	2.952-05	1.595-05
Stainless Steel in first 0.1 m of Central Cell Blanket	1	4.472+01	

Effective Penetration Shield Thickness = 0.1 m

Region	Zone	Al in Magnets	Cu in Magnets
Barrier Coil	9	4.712-01	3.110-01
	10	2.201-01	1.570-01
	11	2.841-01	1.874-01
	12	1.444-01	8.569-02
	13	5.020-02	3.666-02
	14	9.031-03	5.286-03
Transition Coil	19	1.233-04	1.043-04
Stainless Steel in first 0.1 m of Central Cell Blanket	1	4.566+01	

shown for the two cases of 0.1 m and 0.2 m shield thickness. This again identifies the barrier solenoid as an area that needs better shielding, since the ratio of displacement rate there in region IX to the dispacement rates at the central cell is only $\sim 10^{-2}$. It can be noticed that Al sustains higher displacement rates than Cu. As shown in Table IX it will also sustain higher He gas production rates than Cu (although less in terms of H gas production), which may lead to swelling probelms, unless properly shielded.

As a check on our calculations of the required shield thickness in the last section, we use the following more recent equation for the radiation induced resistivity (ρ_r) for Cu:[8]

$$\rho_r = \rho_s(1- e^{-563d}) \ \Omega.m \qquad (20)$$

where: $\rho_s = 3 \times 10^{-9}$ $\Omega.m$, is the saturation resistivity,

d = the total number of displacements.

If we consider a value of ρ_r of 10% of the saturation resistivity for Cu, then:

$$\rho_r = 3 \times 10^{-10} \ \Omega.m \ .$$

This is about a 65% increase in the resistivity of Cu at 80 kG: 4.6×10^{-10} $\Omega \cdot m$, and according to Abdou,[8] requires a change of the conductor surface

Table IX

Gas Production Values in Magnet Components (appm/year).
Effective Penetration Shield Thickness = 0.1 m.

Hydrogen Gas Production

Region	Zone	Al in Magnets	Cu in Magnets
Barrier Solenoid	9	1.712+00	1.924+00
	10	1.504-01	3.407-01
	11	1.845-01	3.280-01
	12	3.108-02	1.616-01
	13	8.940-02	1.397-01
	14	5.516-03	6.780-03
Transition Coil	19	2.549-05	2.995-04
Stainless Steel in first 0.1 m of Central Cell Blanket	1	7.081+02	

Helium Gas Production

Region	Zone	Al in Magnets	Cu in Magnets
Barrier Solenoid	9	7.913-01	2.430-01
	10	6.148-02	2.016-02
	11	8.800-02	2.710-02
	12	1.378-02	4.421-03
	13	3.598-02	1.105-02
	14	2.627-03	7.981-04
Transition Coil	19	4.308-12	0.000+00
Stainless Steel in first 0.1 m of Central Cell Blanket	1	1.673+02	

width by less than 30% to keep the operating current constant. Such modification can practically be done without much difficulty. Thus if:

$$\frac{\rho_r}{\rho_s} = 0.10 = 1 - e^{-563d} \quad ,$$

we get as a value of the allowable dpa in Cu:

$$d_a = 1.871 \times 10^{-4} \text{ dpa} \quad .$$

Concentrating our attention on zone 9 of the barrier solenoid, and in analogy to Eqs. 17 and 18, we can estimate a local dpa attenuation coefficient from:

$$\lambda = \frac{y - x}{2 \ln (d_o/d)} \text{ [m]} \qquad (21)$$

where: d and d_o are the dpa values calculated at the center of two shield thicknesses y and x respectively.

From the results of Table VIII we can estimate λ for zone 9 as:

$$\lambda = \frac{0.2 - 0.1}{2 \ln \frac{3.110 \times 10^{-1}}{8.192 \times 10^{-2}}} = 0.037 \text{ m} \quad ,$$

which is not much different from the value obtained for the scalar flux local attenuation coefficient in zone 9 as: 0.033 m. Again, in analogy to Eq. 19, we can write for the required shield thickness to reduce the dpa to the required value d_a as:

$$y = x + 2\lambda \ln \frac{d_o}{d_a} \quad , \tag{22}$$

which leads to:

$$y = 0.1 + 2 \times 0.037 \ln \frac{3.110 \times 10^{-1}}{1.871 \times 10^{-4}}$$

or: $y = 0.649$ m .

This value pertains to Cu, which was noticed to undergo less displacements than Al. For a conservative design (and since no data were located for Al for an analogous equation to Eq. 25), we obtain the corresponding value for Al as:

$$y' = y \frac{\text{dpa (Al)}}{\text{dpa (Cu)}} = 0.649 \times \frac{4.712 \times 10^{-1}}{3.110 \times 10^{-1}} = 0.983 \text{ m} \quad ,$$

which is not much different from the result obtained in the last section as 1.050 m for Al, and checks the validity of our calculations in the last section depending on two data sources.

IV. Conclusions and Recommendations

We analyzed in this paper the problem of neutron leakage through the end parts of a tandem mirror reactor, and the shielding of the associated magnet system at this position. The central cell, end plug, and associated magnet system were realistically modelled in a three-dimensional way, and the Monte Carlo method was used in the calculations. To get significant contributions at the end-plug components from the central cell neutron source, a method of position dependent angular source biasing was developed, and applied

successfully. The suggested approach may prove useful in similar radiation streaming problems in fusion reactors.

The penetration shield thickness was varied and the required shield thicknesses were determined so as to ensure cryogenic stabilization in the coils. The cylindrical barrier solenoid is identified as requiring careful shielding in the range of 1 m thickness of a steel-lead-boron carbide-water shielding mixture. This shield will also be subjected to a large volumetric neutron heating (5.8 MW/m^3) that is comparable to the one in the blanket at the central cell (8.1 MW/m^3). Thus this part of the shield will need thermal and hydraulic designs similar to those in the central cell. The other magnets in the penetration, however, do not need so much shielding. For example, the first transition coil only needs about 0.2 m of shielding. Another significant result of our study is the estimate of the flux at the direct convertors: 1.3×10^{15} $n/(m^2 \cdot s)$. This is two orders of magnitude lower than that reported[3] at the neutral beam injectors in tokamaks of around 10^{17} $n/(m^2 \cdot s)$. This result stems from the possibility in tandem mirrors of injecting hydrogen ions in the end plug for plasma heating instead of deuterium ions. This avoids the creation of a DT or a DD neutron source in the end plug region. This encouraging result toward solving the radiation streaming problem in this fusion system was arrived at by close collaboration between the plasma and the shielding designers. This is of course possible in other fusion concepts once the radiation streaming problem is clearly identified at an early stage in the design. The lower radiation leakage in this system is perceived as a potential major advantage of tandem mirrors compared to toroidal systems and laser reactor systems. We think it can be further reduced by dumping the leakage neutrons at the end of the mirror into a neutron flux trap, and

directing the charged particles into the direct convertors through flux diverting coils. This idea needs further investigation and would lead to even less neutron leakage and consequently, to minimal activation in the direct convertors.

Acknowledgements

This work was supported by a grant from the U.S. Department of Energy. We thank R. T. Perry and J. Santarius for helpful discussions. The manuscript preparation by Beth Brown is appreciated.

References

1. B. Badger et al., "Preliminary Information on the University of Wisconsin Tandem Mirror Reactor Design," University of Wisconsin, Fusion Engineering Program, UWFDM-325, Nov. 1979.

2. R. W. Moir et al., "Preliminary Design Study of the Tandem Mirror Reactor (TMR)," Lawrence Livermore Laboratory, UCRL-52302, July 1977.

3. J. Jung and M. A. Abdou, "Radiation Shielding of Major Penetrations in Tokamak Reactors," Nuclear Technology 41, 71 (Nov. 1978).

4. M. M. H. Ragheb, A. C. Klein, and C. W. Maynard, "Three-Dimensional Neutronics Analysis of the Mirrors-Beam Duct-Shield System for a Laser Fusion Power Reactor," University of Wisconsin, Fusion Engineering Program, UWFDM-239, April 1978.

5. M. M. H. Ragheb, A. C. Klein, and C. W. Maynard, "Neutronics Shielding Analysis of the Last-Mirrors-Beam Duct System for a Laser Fusion Power Reactor," to appear in Nuclear Technology (1980).

6. Radiation Shielding Information Center, "MORSE-CG," Oak Ridge National Laboratory (1978).

7. W. E. Ford III, R. T. Santoro, R. W. Roussin, and D. M. Plaster, "Modification Number One to the Coupled 100n-21γ Cross Section Library for EPR Calculations," ORNL/TM-5249, Oak Ridge National Laboratory (1976).

8. M. A. Abdou and R. W. Roussin, "MACKLIB 100-Group Neutron Fluence-to-Kerma Factors and Reaction Cross Sections Generated by the MACK Computer Program from Data in ENDF Format," ORNL/TM-3706, Oak Ridge National Laboratory (1976).

9. R. W. Moir, W. L. Barr, and G. H. Miley, "Surface Requirements for Electrostatic Direct Energy Convertors," UCRL-75323, Lawrence Livermore Laboratory, (Jan. 1974).

10. M. M. H. Ragheb, "Optimized Fissile and Fusile Breeding in a Laser-Fusion Fissile-Enrichment Flux Trap Blanket," FSL-2, Fusion Studies Laboratory, Univ. of Illinois (Nov. 1979).

11. M. A. Abdou, "Nuclear Design of the Blanket/Shield System for a Tokamak Experimental Power Reactor," ANL/CTR/TM-51, Argonne National Laboratory (July 1979).